Chapter 2
Magnetic Field Modeling

2.1 Introduction

Magnetic field modeling of the spherical actuator refers to the formulation of magnetic flux density distribution of the PM-pole rotor. There are mainly two purposes for the magnetic field modeling of the spherical actuator. First, torque modeling is necessary for position and velocity control of the spherical actuator. According to Lorentz force law, one prerequisite of the torque modeling is to formulate the magnetic field distribution of the PM-pole rotor analytically. Second, the magnetic field model facilitates the simulation and comprehension of the flux density variation of the PM-pole rotor.

Various magnetic field modeling approaches have been investigated by other researchers. A method based on Maxwell equations has been proposed by Prieto *et al*. [1] to obtain the magnetic component model for planar structures successfully. This method is applicable to one-dimensional (1D) magnetic field, i.e. the magnetic field vector has a constant direction. As an improvement, by using quasi-Poissonian/Laplace's equations in polar coordinates, Zhu *et al*. [2, 3] have developed an analytical technique to predict the 2D magnetic field distribution of single-axis brushless PM machines. Similar approaches have been utilized by Cho *et al*. [4] to analyze the 2D magnetic field of a planar motor, and by Polinder *et al*. [5] to analyze the 2D magnetic field in the cylindrical airgap of a PM generator. For many practical cases, the magnetic field with 3D distribution requires different approaches for modeling. Xiong *et al*. [6] have proposed an analytical method of the magnetic field for a linear PM synchronous machine by using the concept of magnetic charge. A general analysis on the magnetic field of a spherical induction motor was introduced by Davey *et al*. [7] using magnetic vector potential. The analysis properly accounts for the diffusion of the magnetic field with changing frequency and motor speed. Wang *et al*. [8, 9] have proposed 2D/3D magnetic field modeling methods based on Laplace's equation in spherical coordinates for two spherical actuators. In these models, pole arrangements like two or four PM poles and three or four windings, are considered. The rotor is in principle regarded as a sphere entirely consisting

L. Yan et al., *Design, Modeling and Experiments of 3-DOF Electromagnetic Spherical Actuators*, Mechanisms and Machine Science 4,
DOI 10.1007/978-94-007-1646-9_2,

of magnetized rare-earth materials. This approach shows less flexibility in actuator design and system analysis to a certain extent. Prieto *et al*. [10] have presented a procedure to obtain the energy in 3D magnetic structures by applying the *Double 2D* methodology. An accurate model of the magnetic component can be obtained from the magnetic field energy. This approach is based on finite-element analysis (FEA), and thus is not suitable for system control.

The challenge of mathematic modeling of PM-pole rotor in spherical actuators lies in: 1. there are three components of flux density at every point of the 3D space; 2. each of these components varies with respect to the specific locations. In this chapter, an analytical modeling method based on Laplace's equation is proposed for the 3D magnetic field of PM-pole rotor. The PM poles are described by generic variables related to the formulation of the magnetic field. Laplace's equations are formulated for deriving the general solution of magnetic scalar potential. Then the analytical solution of magnetic flux density distribution of the PM-pole rotor is obtained with suitable boundary conditions (BCs). With analytical solution of the magnetic flux density, the influence of structure parameters of the rotor on the magnetic field distribution can be studied.

2.2 Configuration of Rotor Poles

When multiple poles are used in a rotor, the PM poles are arranged along the rotor equator in an alternative polarization pattern. Putting a coil between two PMs as shown in Fig. 2.1(b), one neighboring PM will generate an attraction force with it and the other will generate a repulsion force. The attraction and repulsion will move

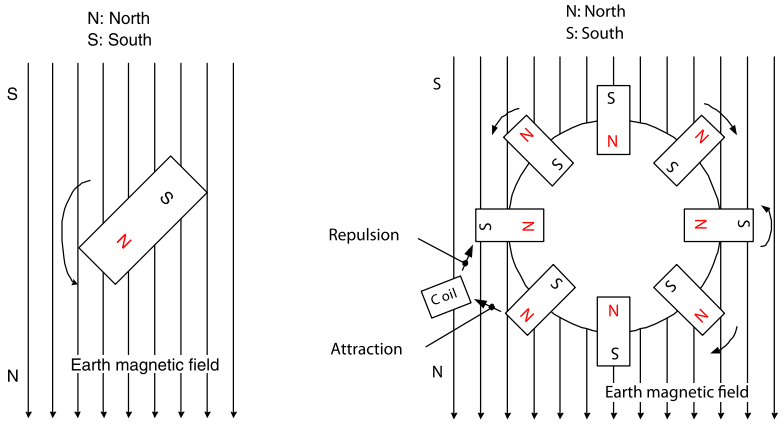

(a) Single PM pole (b) Eight PM poles

Fig. 2.1: Influence of earth magnetic field on rotor poles

the rotor in the same clockwise direction. Therefore, the alternative polarization pattern can achieve larger torque compared with the pattern with same polarization. In order to realize this alternative arrangement in a circle, even number of PM poles are required. Due to the intrinsically high magnetic flux produced by rare-earth magnet as indicated in Fig. 2.1(a), the rotor tends to align itself to the earth magnetic field. This phenomenon is analogous to the effect of earth magnetic field to the compass needle. Having even number of poles distributed uniformly around the equator of the rotor is a method to reduce the inherent self-inducing torque generated by the earth magnetic field at the center of the rotor (Fig. 2.1(b)).

Figure 2.2(a) illustrates the shape of a single rotor pole - an approximated dihedral cone enclosed by *ABCD* and *abcd*. The dihedral cone can be specified by four parameters: longitudinal angle α, latitudinal angle β, rotor radius R_r and rotor core radius R_b. Modeling a single pole as a dihedral cone has several benefits. First, due to the 3-DOF spherical motion of the rotor, the spherical surface of the dihedral-cone-shaped pole can avoid the interference between coils and PM poles, whilst making use of the working space of the rotor completely. Second, the volume of the rotor pole can be specified in spherical coordinates, which facilitates the formulation of the actuator torque. Third, by varying the parameters of the dihedral cone, R_b, R_r, α and β, the study of optimal magnet-pole pattern can be carried out. Figure 2.2(b) presents the PM poles in alternate magnetization directions placed around the equator of the rotor. There are air slots in between PM poles. The regions on top and bottom of the rotor can also be air or low-density materials such as aluminum. These air slots generalize the study of pole arrangement and decreases the inertia moment of the rotor.

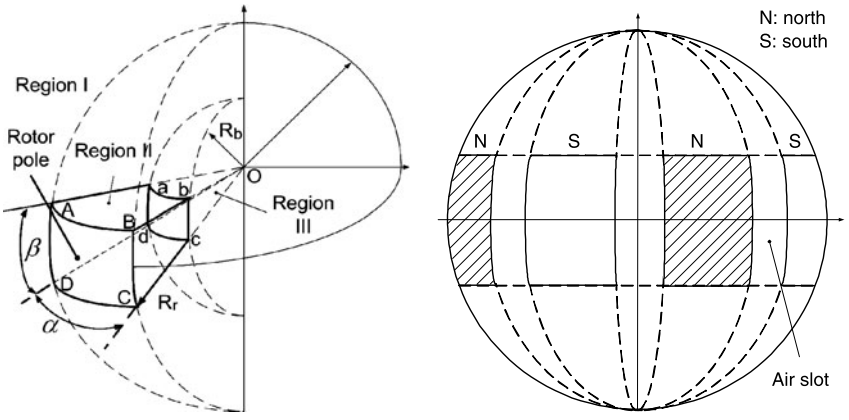

(a) Single rotor pole (b) Alternately arranged rotor pole

Fig. 2.2: Arrangement of rotor poles

2.3 Magnetic Scalar Potential

In the formulation of the magnetic field, the rotor space under study is divided into three regions based on their magnetic characteristics. The air space outside the rotor is denoted as Region *I*. The volume enclosed by *ABCD* and *abcd*, the PM pole (filled with rare-earth magnetic material), is denoted as Region *II*. The inner core enveloped by *abcdo* filled with ferromagnetic materials such as soft iron is denoted as Region *III*. The ferromagnetic core in Region *III* can "converge" the magnetic flux created by PM poles and reduce the magnetic energy loss. It is found that filling Region *III* with magnetized rare-earth material does not have significant improvement on the strength of the magnetic flux density. Rather, the inertia moment of the rotor increases and the dynamic performance of the rotor will be affected.

2.3.1 Relations Between H and B for Three Regions

Region *I* (air) and *III* (iron):

According to the material properties of Region *I* (air) and Region *III* (iron), it is readily to obtain equations relating magnetic field intensity **H** (A/m) to flux density **B** (T) for these two regions [11]:

$$\mathbf{B}_I = \mu_0 \mathbf{H}_I, \tag{2.1}$$

$$\mathbf{B}_{III} = \mu_0 \mu_r \mathbf{H}_{III}, \tag{2.2}$$

where μ_0 is permeability of the free space with a value of $4\pi \times 10^{-7}$H/m, dimensionless quantity μ_r is the relative permeability of soft iron having typical value larger than 4000.

Region *II* (PM):

PM can be characterized by a hysteresis loop which relates **H** to **B**. Figure 2.3(a) presents a typical full hysteresis loop or B-H curve for a rare-earth magnet. From the figure, it can be seen that the variation of **B** always lags behind that of **H**. This phenomenon is called hysteresis of PMs. The second quadrant of the B-H curve, commonly referred to as the demagnetization curve, describes the behavior of magnetic characteristics in actual use. According to Fig. 2.3(b), it can be found that rare-earth magnet exhibits high coercivity and nearly linear demagnetization property. The slope of this demagnetization curve is defined as the recoil permeability μ_{rec} (H/m), or $\mu_0 \mu_m$, where dimensionless quantity μ_m is called relative recoil permeability of magnet having typical value between 1.05 and 1.20. Therefore, for Region *II* (PM) of the rotor, the demagnetization curve can be represented by [11]

$$\mathbf{B}_{II} = \mu_0 \mu_m \mathbf{H}_{II} + \mu_0 \mathbf{M}_0, \tag{2.3}$$

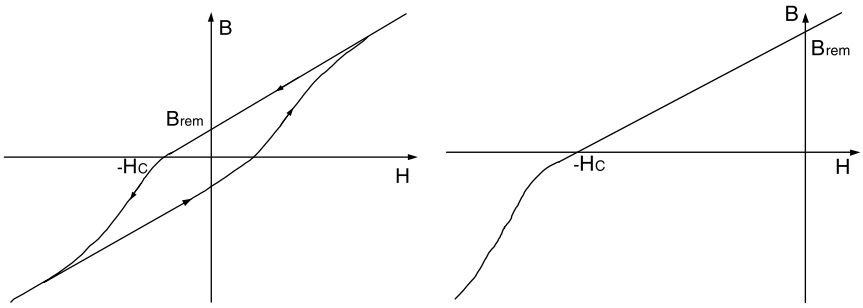

(a) Full hysteresis loop (b) Second quadrant

Fig. 2.3: Typical hysteresis loop of rare-earth magnet

where $\mathbf{M}_0 = \mathbf{B}_{rem}/\mu_0$ (A/m) is the residual magnetization vector and $\mathbf{B}_{rem}$ (T) is remanence of PM.

2.3.2 Laplace's Equations for Three Regions

By using the relations between $\mathbf{H}$ and $\mathbf{B}$ in Eqns. (2.1)-(2.3), Laplace's equations for three regions of the rotor space can be derived as follows.

Magnetic intensity $\mathbf{H}$ vs. scalar potential Φ:

It is known that for three regions of the rotor space, following equation can be obtained [12]

$$\nabla \times \mathbf{H}_i = 0, \tag{2.4}$$

where $i = I$, II and III. Eqn. (2.4) means that $\mathbf{H}_i$ is an irrotational field. According to Helmholtz's theorem [13], the magnetic intensity can be expressed as the gradient of a scalar potential Φ_i, i.e.,

$$\mathbf{H}_i = -\nabla \Phi_i. \tag{2.5}$$

Using the spherical coordinates (r, θ, ϕ), the magnetic field intensity $\mathbf{H}_i$ can be expressed as

$$\begin{aligned}\mathbf{H}_i &= H_{ir}\mathbf{e}_r + H_{i\theta}\mathbf{e}_\theta + H_{i\phi}\mathbf{e}_\phi \\ &= -\left(\frac{\partial \Phi_i}{\partial r}\mathbf{e}_r + \frac{1}{r}\frac{\partial \Phi_i}{\partial \theta}\mathbf{e}_\theta + \frac{1}{r\sin\theta}\frac{\partial \Phi_i}{\partial \phi}\mathbf{e}_\phi\right),\end{aligned}$$

where $\mathbf{e}_r$, $\mathbf{e}_\theta$ and $\mathbf{e}_\phi$ are unit vectors in r, θ and ϕ directions respectively. H_{ir}, $H_{i\theta}$ and $H_{i\phi}$ are three components of the magnetic field intensity $\mathbf{H}_i$, where

$$H_{ir} = -\frac{\partial \Phi_i}{\partial r}, \quad H_{i\theta} = -\frac{1}{r}\frac{\partial \Phi_i}{\partial \theta}, \quad H_{i\phi} = -\frac{1}{r\sin\theta}\frac{\partial \Phi_i}{\partial \phi} \quad . \tag{2.6}$$

According to Maxwell equations [14], a source-free or solenoidal magnetic field has the following property

$$\nabla \cdot \mathbf{B}_i = 0, \tag{2.7}$$

where $i = I$, II and III.

Laplace's equation for outside rotor (Region I):

Outside the rotor (Region I), substituting Eqn. (2.1) into Eqn. (2.5) and Eqn. (2.7), we have

$$\nabla \cdot \mathbf{B}_I = \nabla \cdot (\mu_0 \mathbf{H}_I) = \nabla \cdot [\mu_0(-\nabla \Phi_I)] = 0.$$

Thus,

$$\nabla^2 \Phi_I = 0, \tag{2.8}$$

where ∇^2 is Laplacian operator and Φ_I is the scalar potential in Region I (air).

Laplace's equation for PM (Region II):

Similarly, from Eqns. (2.3), (2.5) and (2.7), following equation can be obtained readily

$$\nabla \cdot \mathbf{B}_{II} = \nabla \cdot [-\mu_0 \mu_m (\nabla \Phi_{II})] + \nabla \cdot (\mu_0 \mathbf{M}_0) = 0,$$

which yields

$$-\mu_m \nabla^2 \Phi_{II} + \nabla \cdot \mathbf{M}_0 = 0,$$

that is

$$\nabla^2 \Phi_{II} = \nabla \cdot \mathbf{M}_0 / \mu_m. \tag{2.9}$$

Eqn. (2.9) is in the form of Poisson's equation. Due to symmetry of the rotor pole arrangement, the divergence of the residual magnetization vector is equal to zero, i.e., $\nabla \cdot \mathbf{M}_0 = 0$. The Poisson's equation can be reduced to Laplace's equation as

$$\nabla^2 \Phi_{II} = 0. \tag{2.10}$$

Laplace's equation for iron core (Region III):

Similar to Region I, scalar potential Φ_{III} of the soft iron core (Region III) can also be obtained as

$$\nabla^2 \Phi_{III} = 0. \tag{2.11}$$

2.3.3 General Solution of Laplace's Equation

In the spherical coordinates, the Laplace's equation can be expressed as

$$\frac{1}{r^2}\frac{\partial}{\partial r}(r^2\Phi_i) + \frac{1}{r^2\sin\theta}\frac{\partial}{\partial\theta}(\sin\theta\frac{\partial\Phi_i}{\partial\theta}) + \frac{1}{r^2\sin^2\theta}\frac{\partial\Phi_i}{\partial\phi} = 0, \tag{2.12}$$

where $i = I, II$ and III, indicating the region of concern. Using separation of variables method, the scalar potential Φ_i can be represented as $\Phi_i(r,\theta,\phi) = R_i(r)\Theta_i(\theta)\Psi_i(\phi)$, where $R_i(r)$, $\Theta_i(\theta)$ and $\Psi_i(\phi)$ are functions of the spherical coordinates. Substituting $\Phi_i(r,\theta,\phi)$ into Eqn. (2.12), the general solution of the scalar potential Φ_i is expressed as [15]

$$\Phi_i = \sum_{n=0}^{\infty}\sum_{m=-n}^{n}[\kappa_{ni}^m r^n + \xi_{ni}^m r^{-(n+1)}][Y_n^m(\theta,\phi)], \tag{2.13}$$

where κ_{ni}^m and ξ_{ni}^m are constants to be determined by boundary conditions. $Y_n^m(\theta,\phi)$ is the spherical harmonic functions defined by

$$Y_n^m(\theta,\phi) = \sqrt{\frac{2n+1}{4\pi}\frac{(n-m)!}{(n+m)!}}[P_n^m(\cos\theta)]e^{im\phi},$$

where $P_n^m(\cos\theta)$ is associated Legendre functions, and n, m are integers with $-n \leq m \leq n$. Note that spherical harmonics are complex valued functions.

2.4 Spherical Harmonic Expansion of M_{0r}

Let M_0 be the magnitude of the residual magnetization vector $\mathbf{M}_0$. With reference to Fig. 2.4 that illustrates the poles placement on the equatorial plane of the rotor, the constituents M_{0r}, $M_{0\theta}$ and $M_{0\phi}$ of $\mathbf{M}_0$ in the directions $\mathbf{e}_r$, $\mathbf{e}_\theta$ and $\mathbf{e}_\phi$ can be computed as

$$M_{0r} = (-1)^{p-1}M_0\cos[\phi - \alpha_0 - \frac{2\pi}{P}(p-1)]\sin\theta, \tag{2.14}$$

$$M_{0\theta} = (-1)^{p-1}M_0\cos[\phi - \alpha_0 - \frac{2\pi}{P}(p-1)]\cos\theta, \tag{2.15}$$

$$M_{0\phi} = (-1)^{p}\ M_0\sin[\phi - \alpha_0 - \frac{2\pi}{P}(p-1)], \tag{2.16}$$

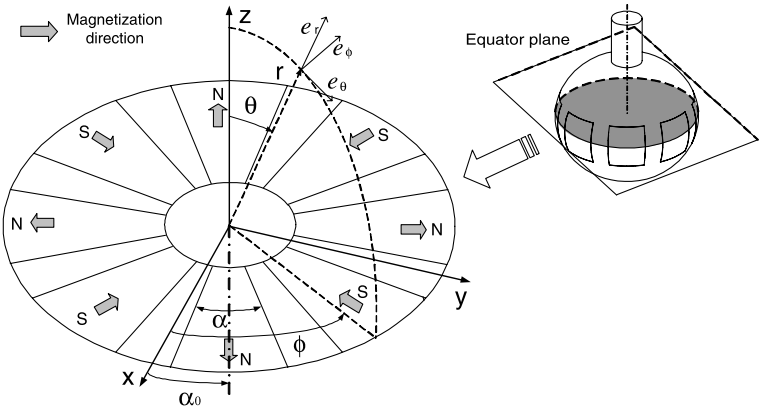

Fig. 2.4: Poles on the equatorial plane of the rotor in spherical coordinates

where $p = 1, 2, ..., P$. P is the total number of PM poles. In this study, $P = 8$, and α_0 is the PM pole angle at the center line in ϕ-direction. Note that these equations are only valid within the range of

$$\frac{\pi}{4}(p-1) + \alpha_0 - \frac{\alpha}{2} < \phi < \frac{\pi}{4}(p-1) + \alpha_0 + \frac{\alpha}{2}, \tag{2.17}$$

$$\frac{\pi}{2} - \frac{\beta}{2} < \theta < \frac{\pi}{2} + \frac{\beta}{2}, \tag{2.18}$$

in the PM pole (Region *II*). For the rest non-magnetized regions in the rotor, the residual magnetization is equal to zero.

When applying boundary conditions to solve the unknowns in the general solution of scalar potential, only the radial component of residual magnetization vector M_{0r} will be used to express the flux density continuity between regions. Components $M_{0\theta}$ and $M_{0\phi}$ do not exist in any boundary condition. The radial component can be expressed as an expansion of spherical harmonic functions $Y_n^m(\theta, \phi)$ as [9]:

$$M_{0r}^s(\theta, \phi) = \sum_{n=0}^{\infty} \sum_{m=-n}^{n} C_{nm} Y_n^m(\theta, \phi), \tag{2.19}$$

where C_{nm} are coefficients determined from the surface integral of the following form:

$$C_{nm} = \int_0^{\pi} \int_0^{2\pi} M_{0r}(\theta, \phi) Y_n^{m*}(\theta, \phi) \sin\theta d\theta d\phi, \tag{2.20}$$

and $Y_n^{m*}(\theta, \phi)$ denotes the complex conjugate of $Y_n^m(\theta, \phi)$. Substituting Eqn. (2.14) into Eqn. (2.20) gives the coefficients

$$C_{nm} = M_0 \int_0^{2\pi} f(\phi) e^{-im\phi} d\phi \int_0^{\pi} \sqrt{\frac{2n+1}{4\pi} \frac{(n-m)!}{(n+m)!}} [P_n^m(\cos\theta)] \sin^2\theta d\theta, \quad (2.21)$$

where

$$f(\phi) = (-1)^{p-1} \cos[\phi - \alpha_0 - \frac{\pi}{4}(p-1)], \; p = 1, 2, ..., 8. \quad (2.22)$$

It is found that $C_{nm} \neq 0$ if and only if $m = \pm 4, \pm 12, \pm 20, ...$ Thus, the fundamental terms of the spherical harmonic functions can be taken at $n = 4$ and $m = \pm 4$. For simplicity, only these terms are used for the derivation of the magnetic field. Denote

$$a \pm bi \equiv \int_0^{2\pi} f(\phi) e^{-im\phi} d\phi \quad (m = 4 \text{ and } m = -4), \quad (2.23)$$

$$c/\sqrt{\pi} \equiv \int_0^{\pi} \sqrt{\frac{2n+1}{4\pi} \frac{(n-m)!}{(n+m)!}} \sin^2\theta [P_n^m(\cos\theta)] d\theta, \quad (2.24)$$

where a, b and c are real numbers. As M_{0r} is available within the range defined by Eqns. (2.17) and (2.18), integrals in Eqns. (2.23) and (2.24) are also constrained by the same range. Out of this range, the integrals are equal to zero. It can be verified that the results of the second integral for $m = 4$ and $m = -4$ are the same. Consequently, the coefficients, $C_{4,4}$ and $C_{4,-4}$, can be obtained based on Eqn. (2.21) as

$$C_{4,4} = M_0 \frac{1}{\sqrt{\pi}} (a + bi) c, \qquad C_{4,-4} = M_0 \frac{1}{\sqrt{\pi}} (a - bi) c, \quad (2.25)$$

where $C_{4,-4}$ is the complex conjugate of $C_{4,4}$. Therefore, the radial component, M_{0r}, of the residual magnetization vector can be expressed in terms of spherical harmonics as

$$M_{0r}^s(\theta, \phi) = C_{4,-4} Y_4^{-4}(\theta, \phi) + C_{4,4} Y_4^4(\theta, \phi), \quad (2.26)$$

where $Y_4^{-4} = 3/16\sqrt{35/2\pi} \sin^4\theta e^{-4i\phi}$ and $Y_4^4 = 3/16\sqrt{35/2\pi} \sin^4\theta e^{4i\phi}$.

2.5 Boundary Conditions

Utilizing the boundary conditions in between different regions of the rotor space as well as the spherical harmonic expansion of M_{0r}, coefficients κ_{nI}^m, κ_{nII}^m, κ_{nIII}^m, ξ_{nI}^m, ξ_{nII}^m and ξ_{nIII}^m, in the general solution of magnetic scalar potential of Eqn. (2.13) can be obtained. Because only the flux density in Region *I* can produce actuator force/torque by interacting with the air-core coils, the coefficients κ_{nI}^m and ξ_{nI}^m are of significant importance.

2.5.1 Boundary Condition A or Far Field Boundary Condition ($B_{Ir}|_{r\to\infty}=0$, $B_{I\theta}|_{r\to\infty}=0$ and $B_{I\phi}|_{r\to\infty}=0$)

The magnetic flux density decreases when the radial distance r increases. Three components of the flux density, B_{Ir}, $B_{I\theta}$ and $B_{I\phi}$ tend to zero when $r\to\infty$. According to Eqns. (2.6) and (2.13), the boundary condition $B_{Ir}|_{r\to\infty}=0$ can be written as

$$\begin{aligned} B_{Ir}|_{r\to\infty} &= -\mu_0\frac{\partial\Phi_I}{\partial r}|_{r\to\infty} \\ &= -\mu_0\sum_{n=0}^{\infty}\sum_{m=-n}^{n}[n\kappa_{nI}^m r^{n-1}-(n+1)\xi_{nI}^m r^{-(n+2)}][Y_n^m(\theta,\phi)]|_{r\to\infty}=0. \end{aligned}$$

Through inspection of the exponential terms, it can be concluded that $\kappa_{nI}^m = 0$. With the aid of Eqns. (2.6) and (2.13), the boundary conditions $B_{I\theta}|_{r\to\infty}=0$ and $B_{I\phi}|_{r\to\infty}=0$ can be expressed as follows.

$$\begin{aligned} B_{I\theta}|_{r\to\infty} &= -\mu_0\frac{1}{r}\frac{\partial\Phi_I}{\partial\theta}|_{r\to\infty} \\ &= -\mu_0\sum_{n=0}^{\infty}\sum_{m=-n}^{n}[\kappa_{nI}^m r^{n-1}+\xi_{nI}^m r^{-(n+2)}]\sqrt{\frac{2n+1}{4\pi}\frac{(n-m)!}{(n+m)!}}\frac{\partial[P_n^m(\cos\theta)]}{\partial\theta}e^{im\phi}|_{r\to\infty} \\ &= 0, \\ B_{I\phi}|_{r\to\infty} &= -\mu_0\frac{1}{r\sin\theta}\frac{\partial\Phi_I}{\partial\phi}|_{r\to\infty} \\ &= -\mu_0\sum_{n=0}^{\infty}\sum_{m=-n}^{n}[\kappa_{nI}^m r^{n-1}+\xi_{nI}^m r^{-(n+2)}]\sqrt{\frac{2n+1}{4\pi}\frac{(n-m)!}{(n+m)!}}\frac{P_n^m(\cos\theta)}{\sin\theta}e^{im\phi}(im)|_{r\to\infty} \\ &= 0. \end{aligned}$$

These two conditions lead to the same result $\kappa_{nI}^m = 0$, as that of $B_{Ir}|_{r\to\infty}=0$.

2.5.2 Boundary Condition B ($B_{Ir}|_{r=R_r}=B_{\text{II}r}|_{r=R_r}$)

On the interface of Region *I* (air) and Region *II* (PM) as shown in Fig. 2.5 (a), the components of the flux density B_{Ir} and $B_{\text{II}r}$ are normal to the interfacial surface of the two neighboring medium. Applying the law of conservation of the magnetic flux [17] to the cylindrical volume in Fig. 2.5 (a) and allowing $\Delta h\to 0$, the result of $B_{Ir}\Delta S = B_{\text{II}r}\Delta S$ can be obtained, hence $B_{Ir}|_{r=R_r}=B_{\text{II}r}|_{r=R_r}$, where R_r is the radius of the rotor that defines the spherical boundary between these two regions.

Projecting all terms of Eqn. (2.3) into the r-direction gives

$$B_{\text{II}r} = \mu_0\mu_m H_{\text{II}r}+\mu_0 M_{0r}. \tag{2.27}$$

Substituting Eqn. (2.19) into Eqn. (2.27), the radial component B_{IIr} of magnetic flux density can be expressed as

$$B_{IIr} = \mu_0 \mu_m H_{IIr} + \mu_0 \sum_{n=0}^{\infty} \sum_{m=-n}^{n} C_{nm} [Y_n^m(\theta, \phi)]. \tag{2.28}$$

By taking advantage of Eqns. (2.6) and (2.13), Eqn. (2.28) is rewritten as

$$\begin{aligned} B_{IIr} = & -\mu_0 \mu_m \sum_{n=0}^{\infty} \sum_{m=-n}^{n} [n \kappa_{nII}^m r^{n-1} - (n+1) \xi_{nII}^m r^{-(n+2)}][Y_n^m(\theta, \phi)]|_{r=R_r} \\ & + \mu_0 \sum_{n=0}^{\infty} \sum_{m=-n}^{n} C_{nm} [Y_n^m(\theta, \phi)]. \end{aligned} \tag{2.29}$$

Therefore, the boundary condition $B_{Ir}|_{r=R_r} = B_{IIr}|_{r=R_r}$ is expanded to

$$\begin{aligned} & -\mu_0 \sum_{n=0}^{\infty} \sum_{m=-n}^{n} [-(n+1) \xi_{nI}^m r^{-(n+2)}][Y_n^m(\theta, \phi)]|_{r=R_r} \\ = & -\mu_0 \mu_m \sum_{n=0}^{\infty} \sum_{m=-n}^{n} [n \kappa_{nII}^m r^{n-1} - (n+1) \xi_{nII}^m r^{-(n+2)}][Y_n^m(\theta, \phi)]|_{r=R_r} \\ & + \mu_0 \sum_{n=0}^{\infty} \sum_{m=-n}^{n} C_{nm} [Y_n^m(\theta, \phi)]. \end{aligned} \tag{2.30}$$

As the spherical harmonics $Y_n^m(\theta, \phi)$ are orthonormal functions [16], Eqn. (2.30) holds for each pair of n and m. The following relation can be subsequently obtained

$$(n+1) \xi_{nI}^m = -\mu_m [n \kappa_{nII}^m R_r^{2n+1} - (n+1) \xi_{nII}^m] + C_{nm} R_r^{n+2}. \tag{2.31}$$

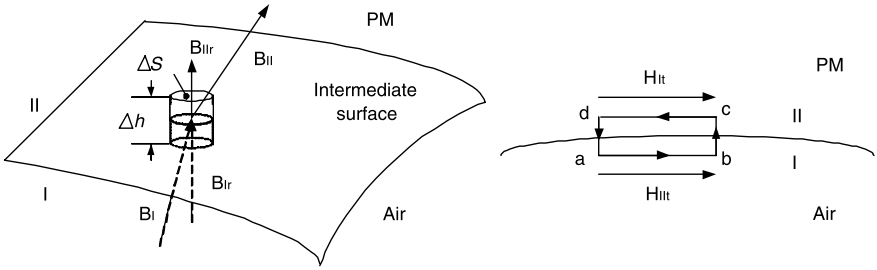

(a) $B_{Ir} = B_{IIr}$ (b) $H_{It} = H_{IIt}$

Fig. 2.5: Continuity boundary conditions

2.5.3 Boundary Condition C ($H_{I\phi}|_{r=R_r} = H_{II\phi}|_{r=R_r}$ and $H_{I\theta}|_{r=R_r} = H_{II\theta}|_{r=R_r}$)

According to Ampere's circuital law [17], the line integral of the magnetic intensity along any closed contour is always equal to the total real current crossing a surface limited by the contour. As shown in Fig. 2.5 (b), a narrow rectangular contour at the boundary surface is indicated by $abcd$. The lengthes of l_{da} and l_{bc} tend to be close to zero. If there is no real surface current on the interface, the result of $H_{IIt}l_{cd} - H_{It}l_{ab} = 0$ can be obtained, i.e., $H_{It} = H_{IIt}$ with $l_{cd} = l_{ab}$, where H_{It} and H_{IIt} are tangent to the surface. For the spherical actuator, there are two components H_θ and H_ϕ of the magnetic field intensity which are tangent to the rotor surface between Region I (air) and Region II (PM). Therefore, $H_{It} = H_{IIt}$ is rewritten as $H_{I\phi}|_{r=R_r} = H_{II\phi}|_{r=R_r}$ and $H_{I\theta}|_{r=R_r} = H_{II\theta}|_{r=R_r}$, where $r = R_r$ defines the boundary surface between Region I (air) and II (PM). From Eqns. (2.6) and (2.13), it can be obtained that

$$H_{I\phi} = -\frac{1}{r\sin\theta}\sum_{n=0}^{\infty}\sum_{m=-n}^{n}\xi_{nI}^{m}r^{-(n+1)}\sqrt{\frac{2n+1}{4\pi}\frac{(n-m)!}{(n+m)!}}[P_n^m(\cos\theta)]e^{im\phi}(im),$$

$$H_{II\phi} = -\frac{1}{r\sin\theta}\sum_{n=0}^{\infty}\sum_{m=-n}^{n}[\kappa_{nII}^{m}r^{n} + \xi_{nII}^{m}r^{-(n+1)}]\sqrt{\frac{2n+1}{4\pi}\frac{(n-m)!}{(n+m)!}}[P_n^m(\cos\theta)]e^{im\phi}(im).$$

Substituting these two equations into the boundary condition of $H_{I\phi}|_{r=R_r} = H_{II\phi}|_{r=R_r}$ yields

$$\xi_{nI}^{m}R_r^{-(n+1)} = \kappa_{nII}^{m}R_r^{n} + \xi_{nII}^{m}R_r^{-(n+1)},$$

that is,

$$\xi_{nI}^{m} = \kappa_{nII}^{m}R_r^{2n+1} + \xi_{nII}^{m}. \tag{2.32}$$

Similarly, the following equations can be obtained for the θ-direction

$$H_{I\theta} = -\sum_{n=0}^{\infty}\sum_{m=-n}^{n}\xi_{nI}^{m}r^{-(n+2)}\sqrt{\frac{2n+1}{4\pi}\frac{(n-m)!}{(n+m)!}}\frac{\partial[P_n^m(\cos\theta)]}{\partial\theta}e^{im\phi},$$

$$H_{II\theta} = -\frac{1}{r}\sum_{n=0}^{\infty}\sum_{m=-n}^{n}[\kappa_{nII}^{m}r^{n} + \xi_{nII}^{m}r^{-(n+1)}]\sqrt{\frac{2n+1}{4\pi}\frac{(n-m)!}{(n+m)!}}\frac{\partial[P_n^m(\cos\theta)]}{\partial\theta}e^{im\phi}.$$

From these two equations, it can be verified that the boundary condition of $H_{I\theta}|_{r=R_r} = H_{II\theta}|_{r=R_r}$ yields the same result as Eqn. (2.32).

2.5.4 Finite Boundary Condition D at $r = 0$ ($B_{\text{III}r}|_{r=0} \neq \infty$, $B_{\text{III}\theta}|_{r=0} \neq \infty$ and $B_{\text{III}\phi}|_{r=0} \neq \infty$)

This boundary condition comes from the fact that it is impossible to achieve an infinite value of flux density. According to Eqns. (2.6) and (2.13), the boundary condition, $B_{\text{III}r}|_{r=0} \neq \infty$, can be written as

$$B_{\text{III}r}|_{r=0} = -\mu_0\mu_r \sum_{n=0}^{\infty}\sum_{m=-n}^{n} [n\kappa_{n\text{III}}^m r^{n-1} - (n+1)\xi_{n\text{III}}^m r^{-(n+2)}][Y_n^m(\theta,\phi)]|_{r=0} \neq \infty.$$

This equation indicates that $\xi_{n\text{III}}^m = 0$. It can be verified that $B_{\text{III}\theta}|_{r=0} \neq \infty$ and $B_{\text{III}\phi}|_{r=0} \neq \infty$ yield the same result.

2.5.5 Boundary Condition E ($B_{\text{II}r}|_{r=R_b} = B_{\text{III}r}|_{r=R_b}$)

This boundary condition is similar to BC-B. Following the same development, BC-E results in

$$\begin{aligned} & -\mu_0\mu_r \sum_{n=0}^{\infty}\sum_{m=-n}^{n} [n\kappa_{n\text{III}}^m r^{n-1}][Y_n^m(\theta,\phi)]|_{r=R_b} \\ = \; & -\mu_0\mu_m \sum_{n=0}^{\infty}\sum_{m=-n}^{n} [n\kappa_{n\text{II}}^m r^{n-1} - (n+1)\xi_{n\text{II}}^m r^{-(n+2)}][Y_n^m(\theta,\phi)]|_{r=R_b} \\ & +\mu_0 \sum_{n=0}^{\infty}\sum_{m=-n}^{n} C_{nm}[Y_n^m(\theta,\phi)], \end{aligned} \tag{2.33}$$

that is,

$$\mu_r n\kappa_{n\text{III}}^m R_b^{2n+1} = \mu_m[n\kappa_{n\text{II}}^m R_b^{2n+1} - (n+1)\xi_{n\text{II}}^m] - C_{nm}R_b^{n+2} \tag{2.34}$$

2.5.6 Boundary Condition F ($H_{\text{II}\phi}|_{r=R_b} = H_{\text{III}\phi}|_{r=R_b}$ and $H_{\text{II}\theta}|_{r=R_b} = H_{\text{III}\theta}|_{r=R_b}$)

Following the same procedure of BC-C, $H_{\text{II}\phi}|_{r=R_b} = H_{\text{III}\phi}|_{r=R_b}$ can lead to

$$\begin{aligned} & -\frac{1}{r\sin\theta}\sum_{n=0}^{\infty}\sum_{m=-n}^{n} (\kappa_{n\text{III}}^m r^n)\sqrt{\frac{2n+1}{4\pi}\frac{(n-m)!}{(n+m)!}}[P_n^m(\cos\theta)]e^{im\phi}(im)|_{r=R_b} \\ = & -\frac{1}{r\sin\theta}\sum_{n=0}^{\infty}\sum_{m=-n}^{n} [\kappa_{n\text{II}}^m r^n + \xi_{n\text{II}}^m r^{-(n+1)}]\sqrt{\frac{2n+1}{4\pi}\frac{(n-m)!}{(n+m)!}}[P_n^m(\cos\theta)]e^{im\phi}(im)|_{r=R_b}, \end{aligned}$$

that is

$$\kappa_{n\mathit{III}}^{m} R_b^{2n+1} = \kappa_{n\mathit{II}}^{m} R_b^{2n+1} + \xi_{n\mathit{II}}^{m}. \tag{2.35}$$

$H_{\mathit{II}\theta}|_{r=R_b} = H_{\mathit{III}\theta}|_{r=R_b}$ also yields the same result.

2.5.7 Solution of Coefficients ξ_{nI}^{m} and κ_{nI}^{m}

So far, the values or relationships of coefficients ξ_{nI}^{m}, $\xi_{n\mathit{II}}^{m}$, $\xi_{n\mathit{III}}^{m}$, κ_{nI}^{m}, $\kappa_{n\mathit{II}}^{m}$ and $\kappa_{n\mathit{III}}^{m}$ have been derived from boundary conditions. Specifically, BC-A and BC-D produce $\kappa_{nI}^{m} = 0$ and $\xi_{n\mathit{III}}^{m} = 0$ respectively; BC-B, BC-C, BC-E and BC-F lead to Eqn. (2.31), (2.32), (2.34) and (2.35) respectively. According to Lorentz force law, only the magnetic field in Region *I* (air) generates actuator torque. Therefore, solutions of ξ_{nI}^{m} and κ_{nI}^{m} are important ($\kappa_{nI}^{m} = 0$). By using Eqns. (2.31), (2.32), (2.34) and (2.35), coefficient ξ_{nI}^{m} can be calculated as follows.

First, multiplying Eqn. (2.35) by $\mu_r n$ and adding into Eqn. (2.34) yield

$$(\mu_r - \mu_m) n \kappa_{n\mathit{II}}^{m} R_b^{2n+1} + [\mu_r n + \mu_m (n+1)] \xi_{n\mathit{II}}^{m} + C_{nm} R_b^{n+2} = 0. \tag{2.36}$$

Substituting $\xi_{n\mathit{II}}^{m}$ in Eqn. (2.32) into Eqn. (2.36) gives

$$\kappa_{n\mathit{II}}^{m} = -\frac{[\mu_r n + \mu_m (n+1)] \xi_{nI}^{m} + C_{nm} R_b^{n+2}}{(\mu_r - \mu_m) n R_b^{2n+1} - [\mu_r n + \mu_m (n+1)] R_r^{2n+1}}. \tag{2.37}$$

From Eqns. (2.32) and (2.37), the following result is obtained

$$\xi_{n\mathit{II}}^{m} = \xi_{nI}^{m} + \frac{R_r^{2n+1} \{[\mu_r n + \mu_m (n+1)] \xi_{nI}^{m} + C_{nm} R_b^{n+2}\}}{(\mu_r - \mu_m) n R_b^{2n+1} - [\mu_r n + \mu_m (n+1)] R_r^{2n+1}}. \tag{2.38}$$

Substituting Eqns. (2.37) and (2.38) into Eqn. (2.31) yields

$$\xi_{nI}^{m} = C_{nm} d_n, \tag{2.39}$$

where

$$d_n = -d_n^{\top} / d_n^{\perp}, \tag{2.40}$$

and

$$\begin{aligned} d_n^{\top} &= R_r^{n+2} + \frac{\mu_m (2n+1) R_b^{n+2} R_r^{2n+1}}{(\mu_r - \mu_m) n R_b^{2n+1} - [\mu_r n + \mu_m (n+1)] R_r^{2n+1}}, \\ d_n^{\perp} &= (\mu_m - 1)(n+1) \\ &\quad + \frac{\mu_m (2n+1)[\mu_r n + \mu_m (n+1)] R_r^{2n+1}}{(\mu_r - \mu_m) n R_b^{2n+1} - [\mu_r n + \mu_m (n+1)] R_r^{2n+1}}. \end{aligned}$$

Particularly, for $n=4$ and $m=\pm 4$, the coefficients of ξ_{4I}^{4} and ξ_{4I}^{-4} can be expressed with $C_{4,4}$ and $C_{4,-4}$ in Eqn. (2.25) as

$$\begin{aligned}\xi_{4I}^{4} &= C_{4,4}d_4 = M_0\frac{d_4}{\sqrt{\pi}}(a+bi)c,\\ \xi_{4I}^{-4} &= C_{4,-4}d_4 = M_0\frac{d_4}{\sqrt{\pi}}(a-bi)c,\end{aligned} \tag{2.41}$$

where

$$d_4 = -d_4^{\top}/d_4^{\perp}, \tag{2.42}$$

and

$$\begin{aligned}d_4^{\top} &= R_r^6 + \frac{9\mu_m R_b^6 R_r^9}{4(\mu_r-\mu_m)R_b^9 - (4\mu_r+5\mu_m)R_r^9},\\ d_4^{\perp} &= 5(\mu_m-1) + \frac{9\mu_m(4\mu_r+5\mu_m)R_r^9}{4(\mu_r-\mu_m)R_b^9 - (4\mu_r+5\mu_m)R_r^9},\end{aligned}$$

2.6 Solutions of Scalar Potential and Flux Density

The derivation of the flux density is performed in the space outside of the rotor (Region *I*), because only the magnetic field in this region is used to compute the motor torque according to Lorentz force law. Substituting the coefficients of ξ_{4I}^{4} and ξ_{4I}^{-4} in Eqn. (2.41) into Eqn. (2.13) and discarding the higher order harmonic terms result in

$$\begin{aligned}\Phi_I &= \xi_{4I}^{-4}r^{-5}[Y_4^{-4}(\theta,\phi)] + \xi_{4I}^{4}r^{-5}[Y_4^{4}(\theta,\phi)]\\ &= M_0\frac{d_4}{\sqrt{\pi}}(a-bi)cr^{-5}\left(\frac{3}{16}\sqrt{\frac{35}{2\pi}}\sin^4\theta e^{-4i\phi}\right) + M_0\frac{d_4}{\sqrt{\pi}}(a+bi)cr^{-5}\\ &\quad\left(\frac{3}{16}\sqrt{\frac{35}{2\pi}}\sin^4\theta e^{4i\phi}\right)\\ &= M_0\frac{3cd_4}{8\pi}\sqrt{\frac{35}{2}}r^{-5}\sin^4\theta(a\cos 4\phi - b\sin 4\phi).\end{aligned} \tag{2.43}$$

Using Eqns. (2.1) and (2.6), the flux density in Region *I* (air) can be obtained

$$B_{Ir} = -\mu_0 \frac{\partial \Phi_I}{\partial r} = \frac{15\mu_0 M_0 c d_4}{8\pi} \sqrt{\frac{35}{2}} r^{-6} \sin^4\theta (a\cos 4\phi - b\sin 4\phi), \tag{2.44}$$

$$B_{I\theta} = -\mu_0 \frac{1}{r} \frac{\partial \Phi}{\partial \theta} = \frac{12\mu_0 M_0 c d_4}{8\pi} \sqrt{\frac{35}{2}} r^{-6} \sin^3\theta \cos\theta (b\sin 4\phi - a\cos 4\phi), \tag{2.45}$$

$$B_{I\phi} = -\mu_0 \frac{1}{r\sin\theta} \frac{\partial \Phi}{\partial \phi} = \frac{12\mu_0 M_0 c d_4}{8\pi} \sqrt{\frac{35}{2}} r^{-6} \sin^3\theta (a\sin 4\phi + b\cos 4\phi). \tag{2.46}$$

2.7 Simplification of Magnetic Field Model

It is worth mentioning that in the derivation of the magnetic field model, a generic Cartesian coordinates system is set up as indicated in Fig. 2.4 (or Fig. 2.6(a)), with angle α_0 specifying the position of PM poles. By letting $\alpha_0 = 0$ as shown in Fig. 2.6(b), the magnetic field model can be simplified. In this case, the x- and y-axes pass through the center of PM poles. Correspondingly, Eqns. (2.14) - (2.16) could be simplified as

$$M_{0r} = (-1)^{p-1} M_0 \cos[\phi - \frac{\pi}{4}(p-1)] \sin\theta, \tag{2.47}$$

$$M_{0\theta} = (-1)^{p-1} M_0 \cos[\phi - \frac{\pi}{4}(p-1)] \cos\theta, \tag{2.48}$$

$$M_{0\phi} = (-1)^{p} \ M_0 \sin[\phi - \frac{\pi}{4}(p-1)], \tag{2.49}$$

which are only valid within the range of

$$\frac{\pi}{4}(p-1) - \frac{\alpha}{2} < \phi < \frac{\pi}{4}(p-1) + \frac{\alpha}{2}, \tag{2.50}$$

$$\frac{\pi}{2} - \frac{\beta}{2} < \theta < \frac{\pi}{2} + \frac{\beta}{2}, \tag{2.51}$$

in the PM pole (Region II). Applying these equations into Eqn. (2.20), it can be verified that the constant b is always equal to zero. Hence, all terms related to b in Eqns. (2.44) - (2.46) vanish. Eqns. (2.44) - (2.46) become

$$B_{Ir} = \frac{15\mu_0 M_0 a c d_4}{8\pi} \sqrt{\frac{35}{2}} r^{-6} \sin^4\theta \cos 4\phi, \tag{2.52}$$

$$B_{I\theta} = -\frac{12\mu_0 M_0 a c d_4}{8\pi} \sqrt{\frac{35}{2}} r^{-6} \sin^3\theta \cos\theta \cos 4\phi, \tag{2.53}$$

$$B_{I\phi} = \frac{12\mu_0 M_0 a c d_4}{8\pi} \sqrt{\frac{35}{2}} r^{-6} \sin^3\theta \sin 4\phi. \tag{2.54}$$

This simplification can facilitate the torque formulation greatly.

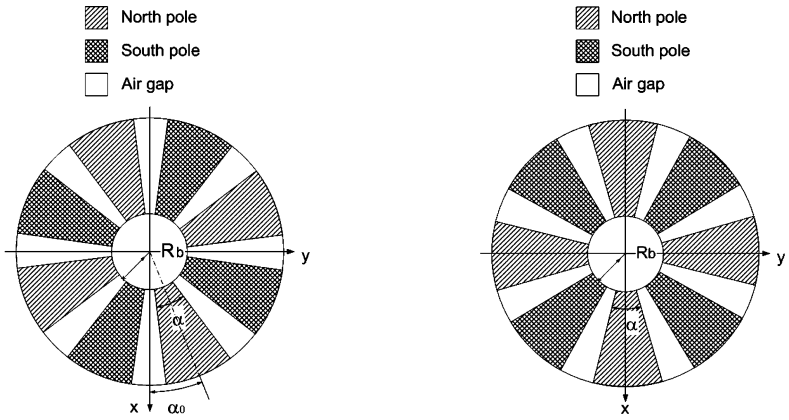

(a) General coordinates (PM pole center specified by α_0)

(b) x-axis through the center of PM pole ($\alpha_0 = 0$)

Fig. 2.6: Coordinates definition in rotor frame

2.8 Summary

This chapter has presented the magnetic field modeling of the PM-pole rotor. According to the magnetic characteristics of the three regions of the rotor space, Laplace's equations of magnetic scalar potential are derived. By using the boundary conditions in between neighboring regions as well as the spherical harmonic expansion of radial component of the residual magnetization vector, coefficients in the general solution of magnetic scalar potential are determined. The magnetic field flux density of the PM rotor is formulated analytically by taking the gradient of the scalar potential. This analytical magnetic field model is described based on the dimensional parameters of the PM poles. Hence, it can be used in the design of the spherical actuator to maximize the torque output.

References

1. Prieto R, Stuchly J A, Cobos J A, Uceda J et al (1999) 1D magnetic component model for planar structures. Proceedings of IEEE International Conference on Power Electronics, vol. 1, no. 27:574–579, Atlanta, USA, June 1999.
2. Zhu Z Q, Howe D, Chan C C et al (2002) Improved analytical model for predicting the magnetic field distribution in brushless permanent-magnet machines. IEEE Transactions on Magnetics, vol. 38, no. 1:229–238, January 2002.
3. Zhu Z Q, Howe D, Bolte E, Ackermann B et al (1993) Instantaneous magnetic field distribution in brushless permanent magnet DC motors, Part I: open-circuit field. IEEE Transactions on Magnetics, vol. 29, no. 1:124–135, January 1993.
4. Cho H S, Im C H, Jung H K et al (2001) Magnetic field analysis of 2-D permanent magnet array for planar motor. IEEE Transactions on Magnetics, vol. 37, no. 5:3762–3766, September 2001.

5. Polinder H, Hoeijmakers M J et al (1997) Analytic calculation of the magnetic field in PM machines. Proceedings of IEEE Industry Applications Society's Annual Meeting, 35–41, New Orleans, Louisiana, USA, 5–9 June 1997.
6. Xiong G, Nasar S A et al (2001) Analysis of fields and forces in a permanent magnet linear synchronous machine based on the concept of magnetic charge. IEEE Transactions on Magnetics, vol. 25, no. 3:2713–2719, May 1989.
7. Davey K, Vachtsevanos G, Powers R et al (1987) The analysis of fields and torques in spherical induction motors. IEEE Transactions on Magnetics, vol. 9, no. 1:273–282, January 1987.
8. Wang J, Jewell G W, Howe D et al (1997) A novel spherical actuator: design and control. IEEE Transactions on Magnetics, vol. 33, no. 5:4209–4211, September 1997.
9. Wang J, Wang W, Jewell G W, Howe D et al (1998) A novel spherical actuator with three degrees-of-freedom. IEEE Transactions on Magnetics, vol. 34, no. 4:2078–2080, July 1998.
10. Prieto R, Cobos J A, Garcia O, Alou P, Uceda J et al (2003) Study of 3-D magnetic components by means of double 2-D methodology. IEEE Transactions on Industrial Electronics, vol. 50, no. 1:183–192, February 2003.
11. Gieras J F, Wing M et al (1998) Permanent Magnet Motor Technology. Marcel Dekker, Inc., New York, 1998.
12. Miner G F (1996) Lines and Electromagnetic Fields for Engineers. Oxford University Press, USA, 1996.
13. Demarest K R (1998) Engineering Electromagnetics. Prentice Hall, Inc., USA, 1998.
14. Solymar L (1976) Electromagnetic Theory. Oxford University Press, UK, 1976.
15. Walter H (1971) Introduction to the Principles of Electromagnetism. Addison-Wesley Publishing Company, Inc., USA, 1971.
16. Virchenko N, Fedotova I et al (2001) Generalized Associated Legendre Functions and Their Applications. World Scientific Publication, USA, 2001.
17. Sadiku N O M (2001) Elements of Electromagnetics. Oxford University Press, UK, 2001.

http://www.springer.com/978-94-007-1645-2

Design, Modeling and Experiments of 3-DOF Electromagnetic Spherical Actuators

Yan, L.; Chen, I.-M.; Lim, C.K.; Yang, G.; Lee, K.-M.

2011, XXI, 163 p., Hardcover
ISBN: 978-94-007-1645-2